Mechanical behaviours of hot-pressed rare-earth oxide (RE = Y and La)-doped TaB_2-SiC composites

Shuqi Guo[#], Gaku Okuma, Kimiyoshi Naito, Hideki Kakisawa

Research Center for Structural Materials, National Institute for Materials Science,
1-2-1 Sengen, Tsukuba, Ibaraki 305-0047, Japan
[#] Corresponding author. E-mail address: GUO.Shuqi@nims.go.jp

Abstract

In this study, TaB_2-20 vol% SiC composites with and without rare-earth oxides (RE_2O_3, RE = Y and La) were fabricated via hot pressing at or above 1800°C. 3 vol% RE_2O_3 additions improved the sinterability of TaB_2-SiC composite and resulted in a finer microstructure in addition to the crystalline $RE_2Si_2O_7$ grain-boundary phase. The shear and Young's moduli as well as hardness of the composites decreased with RE_2O_3 additives. Conversely, the fracture toughness of the composites increased with RE_2O_3 additives and the toughening effect was better for La_2O_3 than for Y_2O_3. On the other hand, the additions of RE_2O_3 substantially enhanced the flexural strength and the strengthening effect was significantly stronger for Y_2O_3 than for La_2O_3, the strengthening was ineffective at or above 1400°C, however. Additionally, the temperature dependence of strengths varied with and without RE_2O_3 additions, as a result of the difference in the chemistry of the intergranular phases.

Keywords: TaB_2; SiC; Rare-earth oxide; Microstructure; Mechanical properties

1. Introduction

Tantalum diboride (TaB_2) belongs to refractory transition metal diborides of the elements of the fifth group of the periodic table and it has the interesting engineering properties like HfB_2 and ZrB_2, e.g. high melting point (>3000°C), high hardness (24.5 GPa), better high temperature mechanical properties, good corrosion resistance, good electrical and thermal conductivity [1–3]. Thus, TaB_2 ceramics are being considered for use in thermal potential components for the metallurgy, microelectronics, absorber for solar energy systems, refractory industries, and more recently, the aerospace filed [4–6]. However, the densification of single phase TaB_2 generally requires very high temperatures (>2000°C) and/or external pressure because of covalent bond and low self-diffusivity [3,7,8]. In addition, although TaB_2 has outstanding properties, its poor oxidation resistance and low mechanical properties restrict its usage in the monolithic form at higher temperatures (>1200°C) [9,10]. Considering the potential application filed, especially enhancing the high temperature properties, such as high temperature strength and oxidation resistance, play an integral role. In order to these, Si-based compositions compounds, like SiC and $MoSi_2$, are the most widely added to single phase TaB_2 to fabricate TaB_2-based ceramic composites [10–15].

Lee et al. [11] prepared a 98.6% dense TaB_2-25.6 vol% SiC composite by reactive hot-pressing (RHP) of the ball-milled Ta, B_4C and Si precursor powders at 1900°C for dwell time of 1 h under a pressure of 32 MPa in Ar atmosphere. The RHP densified TaB_2-25.6 vol% SiC composite had Vickers hardness of 19.1 GPa, Young's modulus of 468 GPa, fracture toughness of 3.35 MPa $m^{1/2}$, and flexural strength of 608 MPa. Unlike monolithic TaB_2 ceramic, passive oxidation protection with parabolic mass gain kinetics was observed for the TaB_2-SiC composite exposed to air at

1500°C, as a result of the formation of a silica-rich glassy layer on the specimen surface. In addition, reactive spark plasma sintering (RSPS) of TaB_2-27.9 vol% SiC composite from mechanically activated Ta, B_4C and Si mixture powder was shown to have relative density of 96% at 1800°C and 20 MPa for 30 min in Ar atmosphere, Vickers hardness of 18.9 GPa and fracture toughness of 8.4 MPa $m^{1/2}$ [12]. The RSPS densified TaB_2-39.1 vol% TaC-13.7 vol% SiC composite had the same density and hardness as the TaB_2-27.9 vol% SiC composite but lowered fracture toughness (4.2 MPa $m^{1/2}$) [13]. Furthermore, Silvestroni et al. [14] obtained a ~95% dense TaB_2-10 vol% $MoSi_2$ composite after hot-pressing of TaB_2-$MoSi_2$ mixture powder at 1680°C for 8 min under a pressure of 30 MPa in vacuum. The resulting TaB_2-10 vol% $MoSi_2$ composite had Vickers hardness of 18.1 GPa, Young's modulus of 535 GPa, fracture toughness of 4.55 MPa $m^{1/2}$ and flexural strength of 630 MPa [14]. However, the strength substantially degraded at elevated temperature in ambient air due to softening of glassy phase in the multiple-grains junctions; the strength decreased to 200 MPa at 1200°C and 100 MPa at 1500°C from 630 MPa at room temperature [14]. Although this composite exhibited sufficient oxidation resistance at 1600°C in static air, its sample completely vaporized during oxidation exposure at 1700°C. On the other hand, a recent study in TaB_2-SiC-$MoSi_2$ composites [15] has shown that the addition of $MoSi_2$ improved anti-oxidation performance of TaB_2-SiC composites, as result of the formation of a dense Ta-Si-B-O glassy layer which blocked oxygen infiltration into the unoxidized bulk material during oxidation exposure. Consequently, it could be expected to develop a TaB_2-based composite with the improved high temperature strength and good oxidation resistance by compositional design and selection.

It is known that RE_2O_3 additives raised the refractoriness and/or the melting point of the protective glassy borosilicate layer that improves the oxidation resistance of ZrB_2- and HfB_2-SiC composites. Jayaseelan et al. [16] had reported significantly improvement of oxidation resistance at 1600°C for ZrB_2-SiC composites with 10 wt% La_2O_3 or Gd_2O_3 additives, owing to the formation of an outermost dense ZrO_2 layer and intermediate layers of heterogeneous $RE_2Si_2O_7$ and amorphous silicate oxides, instead of a porous ZrO_2 layer for ZrB_2-SiC composite without RE_2O_3 additives. Zapata-Solvas et al. [17] had reported that the addition of 2 wt% La_2O_3 improved oxidation resistance of ZrB_2- and HfB_2-SiC composites between 1400°C and 1600°C by increase of glassy borosilicate melt viscosity and decrease of the oxygen diffusion coefficient through the glassy borosilicate melt. In addition, our earlier study in TaC-HfC ceramics has showed that relative density of >98% was obtained for 5 vol% La_2O_3-doped 4TaC-1HfC ceramic after hot pressing at 1750°C [18]. Similarly, nearly fully-dense 4TaC-1ZrC ceramic with 5 vol% La_2O_3 or Y_2O_3 additives (relative density: >99%) was consolidated by hot pressing at a temperature equal to or greater than 1700°C [19]. Furthermore, the obtained RE_2O_3-doped TaC-HfC and TaC-ZrC ceramics showed high fracture strengths at room and elevated temperatures [18,19]. Similar improvement of densification and strength due to Y_2O_3 addition has reported in hot-pressed ZrB_2-SiC composites as well [20]. These earlier investigations have demonstrated that the additions of RE_2O_3 improved not only densification but also high temperature performance and the improvement is closely related to the RE_2O_3 additives.

However, very few studies focused on the characterization of the physical and mechanical properties of TaB_2-SiC composites at room and high temperatures. In particular, studies of strength retention at elevated temperature are rather limited although it is an important high-temperature property for the thermomechanical structural applications of TaB_2-SiC composites. Additionally, to the best of our knowledge, no study about effect of RE_2O_3 additives on the mechanical properties of TaB_2-SiC composites has been reported. This investigation was undertaken to determine the physical and mechanical properties of RE_2O_3-doped TaB_2-SiC composites. TaB_2-20 vol% SiC composites with and without 3 vol% RE_2O_3 (RE = Y and La) additives were fabricated via hot pressing in the temperature range of 1800°C–1900°C. The elastic

properties, hardness and fracture toughness of the resulting highly-dense composites were evaluated at room temperature (RT) and the flexural strength was evaluated in the temperature range of RT–1500°C. The emphasis was to examine the mechanical behaviours at high temperature and effect of RE_2O_3 additions in details.

2. Experimental procedure

2.1 Preparation of composite materials

The raw materials used in this study were: TaB_2 powder (d_{50} = 1.26 μm, Grade-O, Japan New Metals, Osaka, Japan), α-SiC powder (d_{50} = 0.5 μm, UF-15, H.C. Starck, Berlin), Y_2O_3 powder (d_{50} = 1.0 μm, 99.9% purity; Kojundo Chemical Laboratory, Saitama, Japan), and La_2O_3 powder (d_{50} = 1.8 μm, 99.9% purity; Kojundo Chemical Laboratory). Elemental impurities are (wt%): C 0.33, N 0.11 and O 0.25 for the TaB_2 powder; O 1.12, Al 0.02, Fe 0.02 and Ca < 0.01 for the α-SiC powder. Three batches of TaB_2-20 vol% SiC powders with and without 3 vol% RE_2O_3 additives were prepared to examine effects of RE_2O_3 additives on densification and mechanical properties. Hereafter, TaB_2-20 vol% SiC composites with and without 3 vol% Y_2O_3 or La_2O_3 additives are denoted as TS, TS3Y and TS3LA (**Table 1**). The powder mixtures were ball-milled using SiC milling media and ethanol, and the resulting slurry was then dried. Prior to sintering, the dried powders were sieved through a metallic sieve with 60-mesh screen size.

The sintering of the composites was performed by using a hot-pressing apparatus with high-frequency heating (NEW-HP5, Nissin Giken Co., Ltd, Saitama, Japan). The ball-milled powders were loaded into a BN-coated graphite die in rectangularly shaped tablets with dimensions of 21 mm × 25 mm × 3 mm. In the case of TS3Y and TS3LA powders, hot pressing was performed at 1800°C for dwell time of 60 min under an applied pressure of 20 MPa in a flowing Ar atmosphere. In the case of TS powder without RE_2O_3 additives, hot pressing was carried out at different temperatures between 1800°C and 1900°C to obtain a highly-dense sintering compact. The bulk densities of the sintered composites compacts were measured by the Archimedes technique, using distilled water as the medium. The theoretical densities of the composites were calculated on the basis of starting compositions according to the rule of mixture. Density values of 12.57 g/cm^3 for TaB_2, 3.22 g/cm^3 for SiC, 5.03 g/cm^3 for Y_2O_3 and 6.51 g/cm^3 for La_2O_3 were used in the calculation of the theoretical densities. The relative density was determined as the ratio between bulk density and theoretical density.

Table 1 Compositions, theoretical density, bulk density and relative density and phase compositions for the hot-pressed TaB_2-20 vol% SiC composites with and without RE_2O_3 additives.

Materials	Compositions (vol%)				Hot pressing condition	Theoretical density (g/cm^3)	Bulk density (g/cm^3)	Relative density (%)	Phase compositions
	TaB_2	SiC	Y_2O_3	La_2O_3					
TS	80	20	0	0	1800°C/1h/20 MPa/Ar	10.7	9.79	91.5	TaB_2, SiC
					1850°C/1h/20 MPa/Ar	10.7	10.19	95.2	TaB_2, SiC
					1900°C/1h/20 MPa/Ar	10.7	10.3	96.3	TaB_2, SiC
TS3Y	77	20	3	0	1800°C/1h/20 MPa/Ar	10.47	10.06	96.1	TaB_2, SiC, $Y_2Si_2O_7$
TS3LA	77	20	0	3	1800°C/1h/20 MPa/Ar	10.51	10.17	96.7	TaB_2, SiC, $La_2Si_2O_7$

2.2 Characterization

An X-ray diffraction (XRD) was used for identifying the crystalline phases of the sintered composites using the Cu–Kα radiation. Field–emission scanning electron microscopy (FE-SEM, JSM-7001F, JEOL Ltd, Tokyo, Japan) equipped with energy-dispersive spectroscopy (EDS) apparatus was used for microstructural observations and compositional analyses for the resulting highly-dense composites. The grain size, d, of ZrB_2 and SiC phases in the composites was determined by measuring the average linear intercept length, d_m, of the grains in FE-SEM images of the composites, according to the relationship of $d = 1.56d_m$ [21]. The shear modulus, G, Young's modulus, E, and Poisson's ratio, ν, of the composites were calculated using the longitudinal and transverse soundwave velocities which were measured in the specimens [22], by using an ultrasonic equipment (TDS 3052B, Tektronix Inc. Beaverton, OR USA). In addition, the hardness, H, and the fracture toughness, K_{IC}, of the composites were determined using an indentation crack size measurement. The indentation tests were performed on the polished surfaces of the specimens by loading with a Vickers indenter in an automatic hardness testing system (HV-100, Mitutoyo, Co. Ltd., Kawasaki, Japan), with an indentation load of 98 N. The corresponding diagonals of the indentation and crack sizes were measured using an optical microscope attached to the indenter. The fracture toughness of the composites was calculated from the Anstis equation [23].

Test specimens with dimensions of 25 mm × 2.5 mm × 2 mm were cut from the sintered composites compacts. All the specimens were ground with an 800-grit diamond wheel, and the tensile surface for the bend test was polished with diamond paste down to 1.0 µm. The flexural strength was measured in a four-point bending test fixture with inner span of 10 mm and outer span of 20 mm at room temperature (RT), 1000°C, 1200°C, 1400°C and 1500°C in Ar atmosphere. The bending test was performed on an Autograph testing system (AG-X Plus, Shimadzu, Kyoto, Japan) with a loading speed of 0.5 mm/min. For a high-temperature measurement, the specimens were held at the target temperature for 15 min in Ar atmosphere before loading to achieve a uniform temperature distribution. After bending test, the fracture surfaces were observed by FE-SEM.

3. Results and discussion

3.1 Density and microstructure

The densities of the hot-pressed TS, TS3Y and TS3LA compacts at different temperatures between 1800°C and 1900°C are summarized in Table 1. As is evident in this table, for TS powder without RE_2O_3 additives, approximately 92% relative density was obtained at 1800°C and the density increased with increase of sintering temperature, relative density of 96.3% was achieved at 1900°C. A previously study has reported an equal to or higher 97% dense single phase TaB_2 ceramic after hot pressing of a synthesized TaB_2 powder at or above 2000°C for dwell time of 45 min under a pressure of 30 MPa [3]. Compared to the previous study, the addition of SiC significantly improved the sinterability of the single phase TaB_2 ceramic. Improvement of sinterability due to SiC addition has been documented in literature. Lee et al. [11] fabricated a 98.6% dense TaB_2-25.6 vol% SiC composite after hot pressing of mechanically activated Ta, B_4C and Si reactants at 1900°C for dwell time of 1 h under a pressure of 32 MPa in Ar atmosphere. Licheri et al. [12] obtained a 96% dense TaB_2-27.9 vol% SiC composite after RSPS of mechanically activated Ta, B_4C and Si reactants at 1800°C for dwell time of 30 min. In the case of TS3Y and TS3LA powders, on the other hand, relative density of >96% was obtained at 1800°C for dwell time of 60 min under 20 MPa in Ar atmosphere (Table 1), which is the same as that of the TS sample sintered at 1900°C. It is evident that the additions of RE_2O_3 significantly improved the sinterability of TS, and the improvement of densification due to Y_2O_3 additive is the same as

La_2O_3 additive. Improvement of sinterability for non-oxide ceramics due to the additions of RE_2O_3 has been reported elsewhere. Previous studies of SiC showed that to improve sinterability, RE_2O_3 additives are added to SiC, forming an intergranular liquid phase that aids the densification of SiC during sintering [24,25]. In the present study, an intergranular liquid phase is expected in the two compositions, as a result of the reaction of RE_2O_3 with the impurities (SiO_2, Ta_2O_5 etc.) on the initial SiC and TaB_2 particles surfaces during the sintering process. The presence of the intergranular liquid phase favors the process of grain rearrangement as well as improves the packing density of particles, therefore densification.

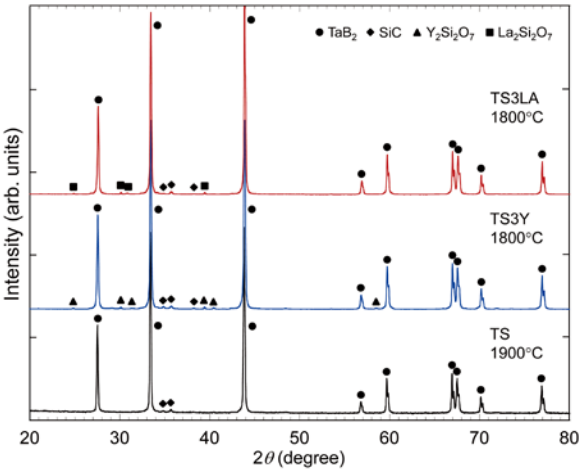

Fig. 1 XRD patterns of the highly-dense TS, TS3Y and TS3LA composites, showing the presence of the crystalline $RE_2Si_2O_7$ grains-boundary phases in TS3Y and TS3LA.

In **Figure 1**, XRD patterns of the hot-pressed TS, TS3Y and TS3LA composites are shown. In the case of TS without RE_2O_3 additives, TaB_2 and SiC phases were detected, with no newly phase. TaB_2 is the primary phase and SiC is the secondary phase. Unlike TS, newly $Y_2Si_2O_7$ and $La_2Si_2O_7$ secondary phases are detected for TS3Y and TS3LA, respectively, in addition to TaB_2 primary phase and SiC secondary phase. However, neither Y_2O_3 nor La_2O_3 phase was detected for TS3Y and TS3LA. The presence of $Y_2Si_2O_7$ or $La_2Si_2O_7$ phase in TS3Y and TS3LA suggests the occurrence of the reactions of Y_2O_3 or La_2O_3 with SiO_2 on the initial SiC powders surface during the sintering process. Similarly, the crystalline $La_2Si_2O_7$ grain-boundary phase was reported in 3 vol% La_2O_3-doped HfB_2-20 vol% SiC composite consolidated by hot-pressing at 2000°C for dwell time of 1 h in Ar atmosphere [26].

It is well-known that the crystalline $RE_2Si_2O_7$ grain boundary phase formed in RE_2O_3-depoed SiC ceramics with the reactions of RE_2O_3 with SiO_2 on the initial SiC particles surface during sintering [24,25]. In the present study, the presence of $RE_2Si_2O_7$ phase in TS3Y and TS3LA should be presumed to be associated with the reactions of RE_2O_3 with SiO_2 on the initial SiC particles surface during the sintering process. However, no products with the reactions of RE_2O_3 with Ta_2O_5 on the initial TaB_2 particles surfaces was detected for each instance (Fig. 1). A previous study has reported that the change in Gibbs free energy, ΔG, for the formation of $La_2Zr_2O_7$ with the reaction of La_2O_3 with ZrO_2 was approximately –151.1 kJ/mol at 1400°C and –152.2 kJ/mol at 1500°C [27]. In comparison, the ΔG value for the formation of $La_2Si_2O_7$ with the reaction of La_2O_3 with SiO_2 was determined to be approximately –2746.7 kJ/mol at 1400°C and –2683.3 kJ/mol at 1500°C. Thermodynamically, thus the formation of $La_2Si_2O_7$ is favored at high temperature compared to the formation of $La_2Zr_2O_7$. Similarly, the thermodynamic feasibility would be expected for the formation of $Y_2Si_2O_7$ with the reaction of Y_2O_3 with SiO_2 during the sintering process. In addition, the study has revealed the formation of $La_2Si_2O_7$ for the ZrB_2-SiC-LaB_6 composite exposed to flowing air at 1500°C, with no $La_2Zr_2O_7$. The absence of $La_2Zr_2O_7$ may be attributed to the significantly low ΔG value of $La_2Si_2O_7$ (–2683 kJ/mol) as compared to that of the former oxide (–152 kJ/mol). Similar cause, although not well-known, would be expected in the RE_2O_3-dopped TaB_2-SiC composites investigated in this study. In addition, a residual intergranular glassy impurity phase should be present for the two composites accompanying the crystallization of $RE_2Si_2O_7$ phase at the grain-boundaries during the sintering

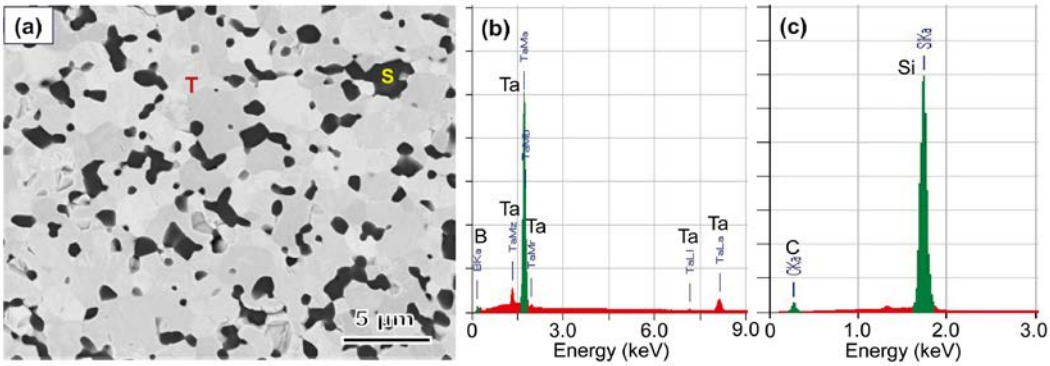

Fig. 2 (a) Backscattered FE-SEM image of the microstructure for TS, (b) and (c) EDS spectrum derived from the grey contrast phase and dark contrast phase respectively marked by symbols T and S in (a).

process, owing to difficult completely crystallization of the intergranular glassy impurity phase. Although the intergranular glassy impurity phase present in the composites is not substantial, in terms of the volume that it occupies, it has a significant, even overriding, effect on the high-temperature mechanical properties of the composites.

Figure 2 shows backscattered electron FE-SEM image of the microstructures of TS without RE_2O_3 additive. As is evident in Fig. 2a, the TS composite consisted of grey contrast phase and dark contrast phase. EDS spectrum derived from the region marked by symbol **T** in Fig. 2a shows that the grey contrast phase consists of Ta and B elements (Fig. 2b). Unlike the grey contrast phase, EDS spectrum derived from the region marked by symbol **S** in Fig. 2a reveals that Si and C elements are present in the dark contrast phase (Fig. 2c). Previous studies had shown that the sintered TaB_2-SiC composite consisted of only TaB_2 and SiC after hot-pressing of the commercially available TaB_2 and SiC powders at 1900°C for 1 h [10] or after RSPS of the synthesized TaB_2-SiC mixture powder at 1800°C for 30 min [12]. Combining with the results of XRD analysis (Fig. 1) and EDS analysis (Fig. 2), thus the grey contrast phase and the dark contrast phase in the TS composite are presumed to be TaB_2 and SiC, respectively. For TS3Y and TS3LA composites, on the other hand, a dark-grey contrast phase was observed at TaB_2/SiC grains-boundaries (indicated by arrows in **Fig. 3** and **Fig. 4**), in addition to equiaxed TaB_2 grains (grey contrast) and SiC grains (dark contrast). EDS analysis reveals that the dark-grey contrast phase consisted of Y, Si and O elements for TS3Y (Fig. 3) and La, Si and O elements for TS3LA (Fig. 4). On the basis of the XRD analysis (Fig. 1) and EDS analysis (Figs. 3 and 4), it is presumed that the dark-grey contrast phase in TS3Y and TS3LA is the crystalline $Y_2Si_2O_7$ and $La_2Si_2O_7$ grain-boundary phases, respectively. In addition, it is found that SiC particles are homogeneously dispersed in the TaB_2 matrix, with no the agglomeration of SiC particles (Figs. 2–4). The measured grain sizes of TaB_2 and SiC phases for the three compositions TS, TS3Y and TS3LA composites are summarized in **Table 2**. As is evident in this table, the grain sizes of TaB_2 and SiC phases are significantly larger for TS than for TS3Y and TS3LA. In comparison, the TaB_2 and SiC grain sizes measured in the TS, TS3Y and TS3LA composites are substantially smaller than those reported in single phase TaB_2 ceramic (TaB_2: 3.6 μm at 2000°C and 5.3 μm at 2100°C [3]) after hot pressing of a synthesized TaB_2 powder (TaB_2 powder: 0.4 μm) at or above 2000°C for 45 min under a pressure of 30 MPa as well as in TaB_2-27.9 vol% SiC composite after RSPS of mechanically activated Ta, B_4C and Si at 1800°C for dwell time of 30 min [12]. Apparently, the additions of Y_2O_3 and La_2O_3 effectively inhibited the rapid grain growth of TaB_2 and SiC phases during the sintering process. The hindering effect of Y_2O_3 and La_2O_3 additives on grain growth is associated with the lowered sintering temperature and/or the formation of the crystalline $Y_2Si_2O_7$

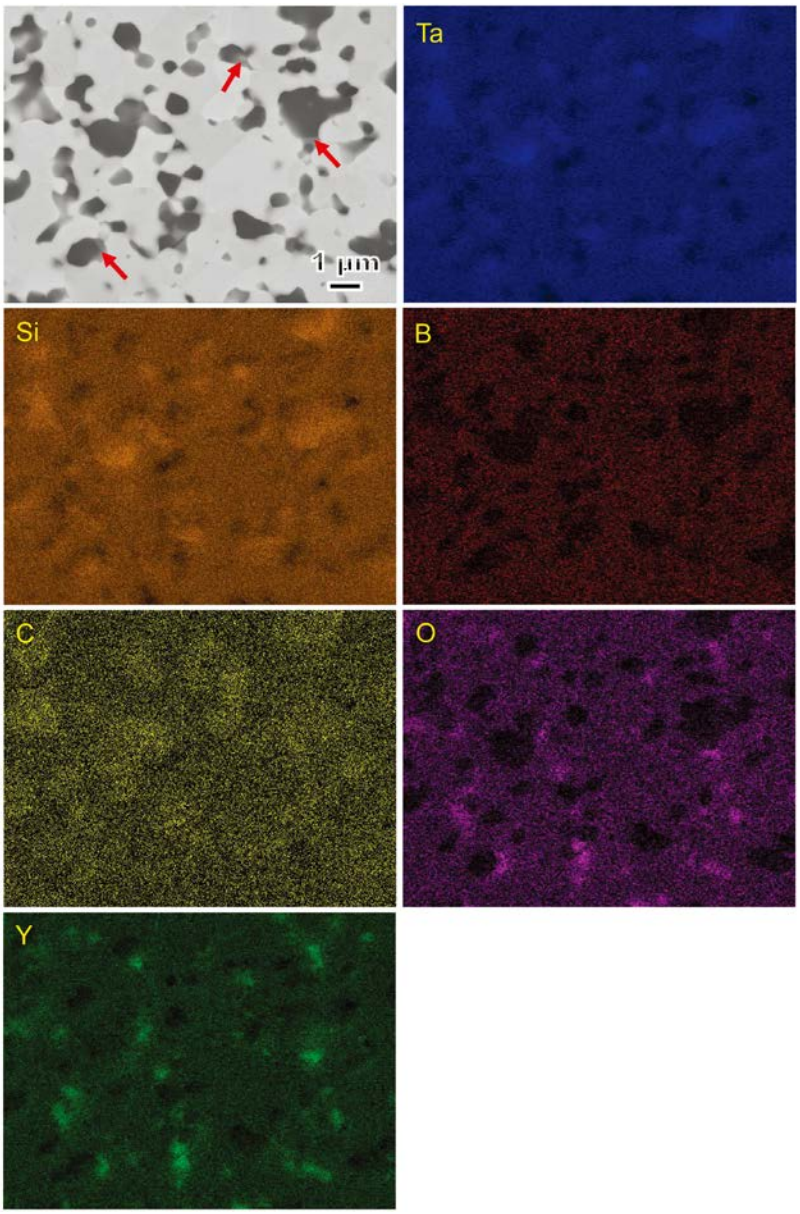

Fig. 3 Backscattered FE-SEM image of the microstructure for TS3Y and the corresponding X-ray elemental distribution maps.

and $La_2Si_2O_7$ secondary phases during the sintering process because their formation reduced the oxide impurities on the initial SiC particles surfaces.

3.2 Elastic and mechanical properties

(a) Elastic properties: The shear modulus, G, Young's modulus, E, and Poisson's ratio, ν, of the TS, TS3Y and TS3LA composites were summarized in Table 2 as well. The shear modulus, Young's modulus and Poisson's ratio were determined to be G = 228 GPa, E = 537 GPa and ν = 0.17 for TS; G = 215 GPa, E = 503 GPa and ν = 0.19 for TS3Y; G = 212 GPa, E = 506 GPa and ν = 0.19 for TS3LA. Apparently, the shear and Young's moduli of TS without RE_2O_3 additives are higher than those of TS3Y and TS3LA, however, the Poisson's ratio is lower for TS than for TS3Y and TS3LA. This discrepancy of the elastic properties due to the additions of RE_2O_3 is associated with the presence of the crystalline $RE_2Si_2O_7$ grain-boundaries phase in TS3Y and TS3LA (Figs. 1–4). In addition, the Young's modulus of TS, TS3Y and TS3LA is lower than that of a 98% dense

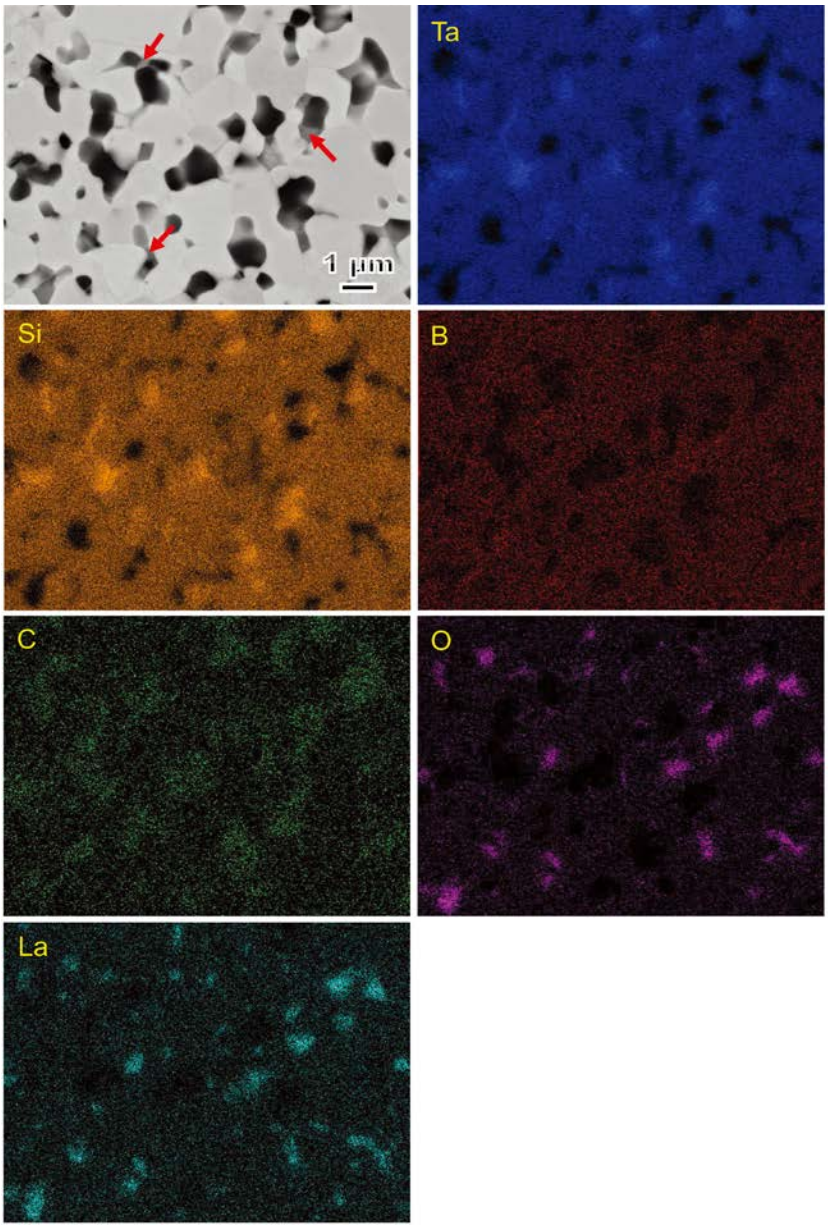

Fig. 4 Backscattered FE-SEM image of the microstructure for TS3LA and the corresponding X-ray elemental distribution maps.

single phase TaB_2 ceramic (E = 551 GPa) after hot pressing of a synthesized TaB_2 powder at 2000°C for dwell time of 45 min under a pressure of 30 MPa [3], but is higher than that of a 98.6% dense TaB_2-25.6 vol% SiC composite (E = 468 GPa) after hot pressing of mechanically activated Ta, B_4C and Si reactants at 1900°C for dwell time of 1 h under a pressure of 32 MPa in Ar [11]. Furthermore, the shear modulus of TS, TS3Y and TS3LA is comparable to that of single phase TaB_2 ceramic (G = 228 GPa [3]) and ZrB_2-20 vol% SiC composite (G = 217–225 GPa [28]). In comparison, the Young's modulus of TS is higher than that of ZrB_2–20 vol% SiC composite (E = 494–512 GPa [28]), but is comparable to that of HfB_2-20 vol% SiC (E = 544 GPa [29]) and TaB_2-10 vol% $MoSi_2$ composites (E = 535 GPa [14]). Unlike TS without RE_2O_3 additives, the Young's modulus of TS3Y and TS3LA is lower than that of HfB_2-20 vol% SiC composite (E = 544 GPa [29]), but is comparable to that of ZrB_2-20 vol% SiC composite (E = 494–512 GPa [28]). In contrast, the Poisson's ratio of TS, TS3Y and TS3LA is higher than that of ZrB_2-20 vol% SiC (ν = 0.14 [28]) and HfB_2-20 vol% SiC composites (ν = 0.12 [30]).

Table 2 Grain size, shear modulus, Young's modulus, Poisson's ratio, hardness, fracture toughness and room-temperature four-point flexural strength for the highly-dense TaB_2-20 vol% SiC composites with and without RE_2O_3 additives.

Materials	Hot pressing condition	Relative density (%)	Grain size, d (μm)		Elastic properties			Hardness, H (GPa)	Fracture toughness, K_{IC} (MPa $m^{1/2}$)	Flexural strength, σ_{RT} (MPa)
			TaB_2	SiC	G (GPa)	E (GPa)	ν			
TS	1900°C/1h/20 MPa/Ar	96.3	1.95 ± 0.91	1.08 ± 0.47	228	537	0.17	23.1 ± 0.5	4.51 ± 0.54	559.3 ± 107.6
TS3Y	1800°C/1h/20 MPa/Ar	96.1	1.46 ± 0.58	0.79 ± 0.37	215	503	0.19	21.9 ± 0.4	4.61 ± 0.35	768.7 ± 50.1
TS3LA	1800°C/1h/20 MPa/Ar	96.7	1.34 ± 0.55	0.85 ± 0.38	212	506	0.19	21.1 ± 0.6	5.01 ± 0.36	625.9 ± 51.6

(b) Hardness and fracture toughness: The hardness of the TS, TS3Y and TS3LA composites were summarized in Table 2 as well. It is found that the hardness of TS without RE_2O_3 additives is higher that of TS3Y and TS3LA, and the hardness value is slightly lower for TS3LA than for TS3Y. It is known that the hardness of monolithic TaB_2 (H = 24.5 GPa) and SiC (H = 23 GPa) is much higher that of $RE_2Si_2O_7$, e.g. H = 6.2 GPa for $Y_2Si_2O_7$ [31]. The low hardness of the intergranular phase suggests that the resistance to intergranular sliding is lower for TS3Y and TS3LA than for TS. Presumably, the lower hardness of TS3Y and TS3LA is associated with the presence of the intergranular $RE_2Si_2O_7$ phase. In comparison, the hardness values of the three compositions are higher than those of a 96% dense TaB_2-27.9 vol% SiC composite (H = 18.9 GPa [12]) and a 98.6% dense TaB_2-25.6 vol% SiC composite (H = 19.1 GPa [11]) as well as TaB_2-10 vol% $MoSi_2$ composite (H = 18.1 GPa [14]), however, they are lower than that of a 97% dense single phase TaB_2 ceramic (H = 25.6 GPa [3]). In addition, the hardness values of TS, TS3Y and TS3LA are comparable to those of HfB_2-20 vol% SiC and ZrB_2-20 vol% SiC composites [28,29].

On the other hand, the fracture toughness measured in TS3Y and TS3LA is larger than that in TS without RE_2O_3 additives (Table 2). Among the three compositions composites, a maximum fracture toughness value of 5.01 ± 0.36 MPa $m^{1/2}$ was obtained for TS3LA. In addition, the fracture toughness of TS and TS3Y is comparable to that of single phase TaB_2 ceramic (K_{IC} = 4.5 MPa $m^{1/2}$ [3]) and TaB_2-10 vol% $MoSi_2$ composite (K_{IC} = 4.55 MPa $m^{1/2}$ [14]). Furthermore, the fracture toughness values obtained in TS, TS3Y and TS3LA are comparable to those reported in HfB_2- and ZrB_2-based with SiC composites [28,29].

The crack propagation behaviour of the three compositions composites was examined under FE-SEM observations, examples of which are shown in **Figure 5**. In the case of TS without RE_2O_3 additives (Fig. 5a), the crack propagated across TaB_2 phase and larger SiC phase, while the crack deflection occurred at the small individual SiC particles (indicated by

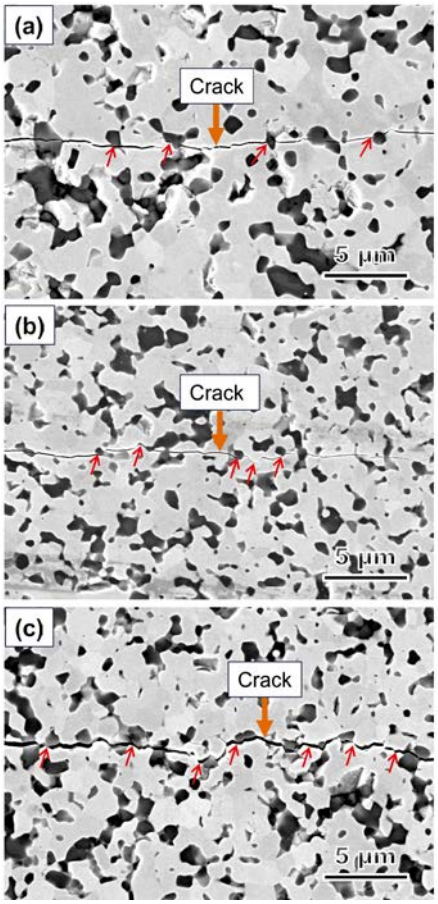

Fig. 5 Examples of crack propagation behaviour in (a) TS, (b) TS3Y and (c) TS3LA.

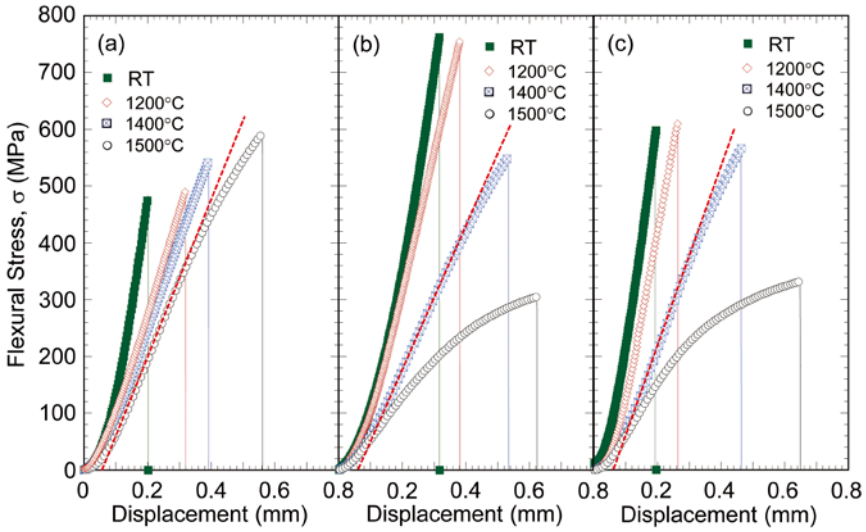

Fig. 6 Typical stress–displacement curves obtained during the bending tests at room and elevated temperatures for (a) TS, (b) TS3Y and (c) TS3LA.

arrows in Fig. 5a). It is known that the contribution of crack deflection to increase fracture toughness depends on the total number of crack deflection and the crack propagation path length. As a result, the crack deflection, that occurred at the small individual SiC particles, is insignificantly contributed to increase fracture toughness of TS, therefore, the comparable fracture toughness with single phase TaB_2 ceramic. Unlike TS, in the case of TS3Y and TS3LA, the crack deflection occurred not only at the small individual SiC particles but also at the TaB_2 particles (indicated by arrows in Fig. 5b and c), which in turn led to an increase of crack propagation path, therefore contributing to increase fracture toughness. For TS3LA (Fig. 5c), particularly, the number of crack deflection and the crack propagation path length significantly increased compared to TS and TS3Y, therefore the highest fracture toughness (Table 2). The difference in the crack behaviour for the three compositions composites is related to the intergranular bonding that involves the chemistry of the intergranular phases. Our earlier studies in HfB_2-SiC and ZrB_2-SiC had shown that the intergranular glassy phase is always presented in the sintered composites, as a result of reactions of the oxide impurities on the raw powder particles surfaces during sintering [32,33]. Similar intergranular glassy phase, although not well-known, could be expected in the three compositions composites investigated in this study. Furthermore, a previously study in hot-pressed SiC ceramic with Al_2O_3 + RE_2O_3 additives (RE = Y, Yb, La, Nd) [34] showed that an increase in the cationic radius of RE_2O_3 was accompanied by a decrease in Young's modulus and hardness as well as an increase in fracture toughness. The effects of the cationic radius of RE_2O_3 on these properties are attributed to the formation of a stronger intergranular glassy phase because the smaller RE^{3+} ions made the intergranular glassy network become more compact and tighter. Because the ionic radius of La^{3+} is larger than that of Y^{3+}, similar cause would be expected for a higher fracture toughness in TS3LA than in TS3Y.

(c) Mechanical behaviour: In **Figure 6**, the stress–displacement curves obtained during the bending tests at room and elevated temperatures for the three compositions composites are presented. In the case of TS without RE_2O_3 additives (Fig. 6a), the stress–displacement curves are linear to failure at or below 1400°C, with no nonlinear deformation. At 1500°C, however, the initial linear response is followed by nonlinear deformation behaviour prior to fracture. Unlike TS, in the case of TS3Y and TS3LA, a little nonlinear deformation prior to failure was observed in the curves obtained at 1400°C (Fig. 6b and c), regardless of the RE_2O_3 additives. At 1500°C, the transition of the stress–displacement curves from linear to nonlinear behaviour initiates at a

considerably lower stress of ~170 MPa for TS3Y and TS3LA (Fig. 6b and c), accompanied a considerable large nonlinear deformation prior to fracture. The nonlinear deformation behaviour at high temperatures has been reported in ZrB_2-20 vol% SiC and HfB_2-20 vol% SiC composites where the nonlinear deformation was observed only at 1600°C [32,33], as a result of the softening of intergranular glassy phase. Apparently, the temperature of the transition from linear to nonlinear behaviour is lower for TaB_2-20 vol% SiC composites with and without RE_2O_3 additives than for ZrB_2-20 vol% SiC and HfB_2-20 vol% SiC composites. This comparison suggests that the intergranular glassy phase is more refractory for ZrB_2-20 vol% SiC and HfB_2-20 vol% SiC composites than for the three compositions TS, TS3Y and TS3LA composites. In addition, the resistance to softening of the intergranular glassy phase for TS was higher than that for TS3Y and TS3LA; this suggests that the RE_2O_3 additives led to degradation of the intergranular glassy phase at high temperature and/or to increase of the amount of this phase. The major cause of the lower resistance to softening of the intergranular glassy phase for TS3Y and TS3LA is not fully understood but may be associated with the difference in the chemistry of the intergranular glassy phase in the three compositions composites.

Figure 7 shows the temperature dependence of the flexural strength for the three compositions composites. In comparison, dada reported elsewhere for ZrB_2-20 vol% SiC and HfB_2-20 vol% SiC composites were also included in this figure. As is evident in this figure, room and high temperature strengths of the three compositions composites are strongly depended on the RE_2O_3 additives. Room temperature flexural strength was determined to be ~495 MPa for TS, ~625 MPa for TS3LA, and ~769 MPa for TS3Y. Apparently, the additions of Y_2O_3 and La_2O_3 significantly increased the strength of TS. A maximum strengthening effect was obtained for TS3Y. In addition, the strength of TS is lower than that of HfB_2-20 vol% SiC [32], but is comparable to that of ZrB_2-20 vol% SiC [35]. Although the strength of TS3LA is comparable to that of HfB_2-20 vol% SiC, the strength of TS3Y is substantially greater than that of HfB_2-20 vol% SiC. Previously studies in ZrB_2-SiC composites showed that smaller starting SiC particles led to finer grains and higher strength [33,36,37] and the largest SiC grains in the microstructure acted as the critical flaws causing the failure of the composite [38]. Furthermore, a previous study in SiC with Al_2O_3 + RE_2O_3 additives (RE = Y, Yb, La, Nd) [34] revealed that the smaller RE^{3+} ions made the glassy network become more compact and tighter, consequently produced a stronger intergranular phase, resulting higher room temperature strength. In the present study, thus the increase of strength due to the additions of RE_2O_3 is attributed to smaller SiC grains (Table 2) and stronger intergranular bonding. The highest fracture strength was obtained for TS3Y, as a result of the smallest SiC grains (Table 2) and smaller Y^{3+} ion radius compared to La^{3+} ion radius for TS3LA. However, the improvement of strength due to the additions of RE_2O_3 is ineffective at or above 1400°C (Fig. 7), as a result of softening of the intergranular glassy phase.

Moreover, the temperature dependence of flexural strength differs for three compositions TS, TS3Y and TS3LA composites (Fig. 7), depended on the RE_2O_3 additives. In the case of TS without RE_2O_3 additives, the flexural strength was constant between RT and 1200°C, independent of the test temperature. Beyond 1200°C, however, the flexural strength increased to 550 MPa at 1400°C and 580 MPa at 1500°C from 495 MPa at RT, respectively,

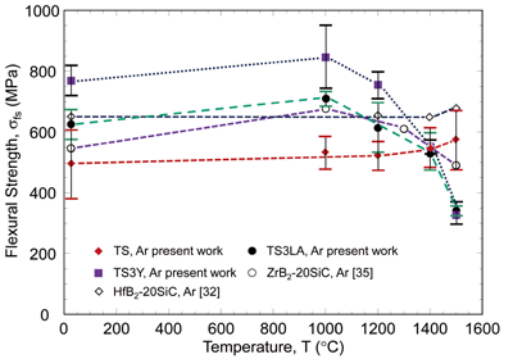

Fig. 7 Plots of flexural strength as a function of test temperature for the TS, TS3Y and TS3LA composites. In comparison, data reported elsewhere for ZrB_2-20 vol% SiC and HfB_2-20 vol% SiC composites are also included.

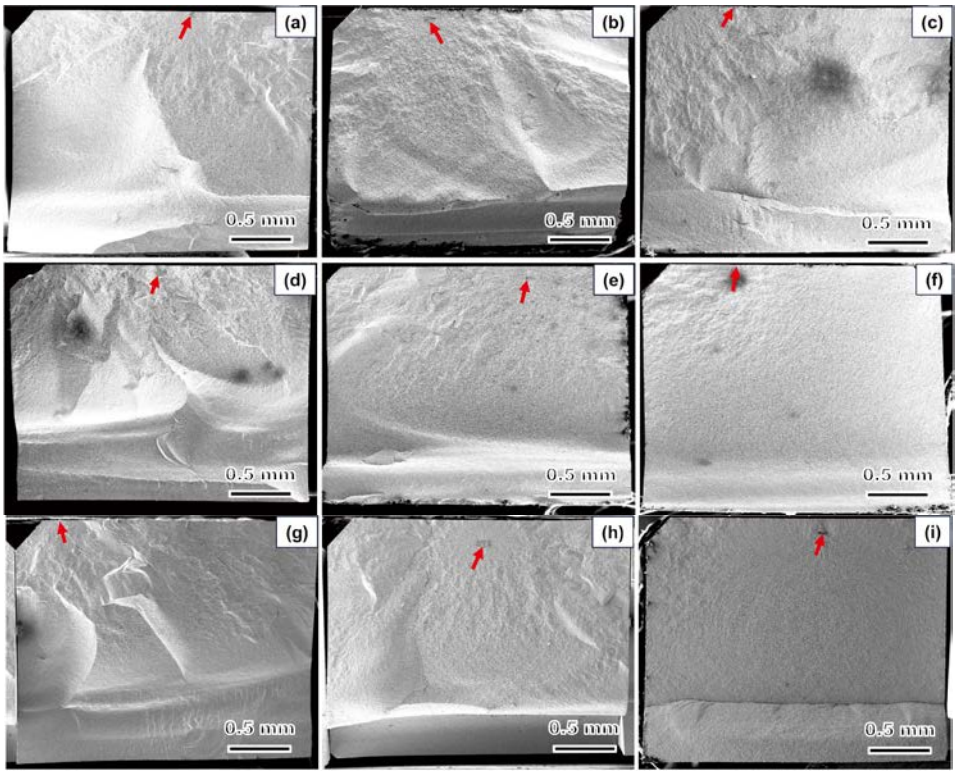

Fig. 8 FE-SEM images of the macro-appearance of the fracture surfaces for the (a–c) TS, (d–f) TS3Y and (g–i) TS3LA composites tested at (a, d, g) RT, (b, e, h) 1400°C and (c, f, i) 1500°C.

for strength increases of ~11% and ~17%. Similar increase of strength was reported for HfB_2-20 vol% SiC and ZrB_2-30 vol% SiC composites at or above 1400°C [32,39]. The increase of strength is attributed to the plastic flow of the materials, which accompanies the stress relief, allowing for an increase in the strength in this temperature regime. Similar cause would be expected for TaB_2-20 vol% SiC composite investigated in this study. However, the strength of TS is lower than that of HfB_2-20 vol% SiC and ZrB_2-20 vol% SiC composites up to 1500°C [32,35]. One exception is higher strength at 1500°C for TS than for ZrB_2-20 vol% SiC composite [35].

In the case of TS3Y and TS3LA, on the other hand, similar temperature dependence of strength was observed regardless of the type of RE_2O_3 additives (Fig. 7). Unlike TS, the flexural strength increased to 850 MPa at 1000°C from 769 MPa at RT for TS3Y and to 711 MPa at 1000°C from 626 MPa at RT for TS3LA, and then the strengths decreased with increase of temperature up to 1500°C. This increase in strength is probably attributed to the relaxation of larger residual internal radial tensile stresses in the triple-grain junctions induced during the crystallization of $RE_2Si_2O_7$ phase. Although the flexural strength below 1400°C is higher for TS3Y than for TS3LA, their strengths are comparable at or above 1400°C. The higher strength for TS3Y below 1400°C is presumed to be associated with smaller Y^{3+} ionic radius for Y_2O_3 because the smaller ionic radii produce a stronger grain boundary phase that contributes to a greater strength [40]. However, this strengthening effect is ineffective at or above 1400°C. This implies that the flexural strength at or above 1400°C is mostly dominated by softening of the intergranular glassy phase. In addition, the flexural strength below 1400°C is higher for TS3Y and TS3LA than for TS. At or above 1400°C, however, the strength of TS3Y and TS3LA is equal to or lower than that of TS. Watts et al. [41] has reported that the thermal residual stresses in ZrB_2-SiC composites were completely relaxed at ~1400°C; thus, substantially degradation of strength for TS3Y and TS3LA above 1400°C indicated that the intergranular bonding is much weaker for TS3Y and TS3LA than for TS due to softening of the intergranular glassy phase.

Figure 8 shows the macro-appearances of the fracture surfaces for the post-test TS, TS3Y and TS3LA composites at room and elevated temperatures. It is seen that the fracture origin was located at the surface flaws and/or at subsurface flaws (indicated by arrows in Fig. 8). The fracture macro-topographies of the specimens differ for the three compositions TS, TS3Y and TS3LA composites. In the case of the TS composite without RE_2O_3 additives, the fracture macro-topographies are essentially similar for all the specimens tested at room and elevated temperatures; the rough fracture surfaces were observed at different temperatures between RT and 1500°C (Fig. 8a–c). The fracture surfaces exhibited three different characteristic regions as follows: (i) slow crack growth (SCG) region, (ii) rapid crack growth region, and (iii) final fracture region. The presence of these characteristic regions suggests that after the crack originates at the flaws of specimen, the slow crack growth is followed by rapid crack growth and final failure due to overload.

The fracture surfaces of the post-test TS specimens at room and high temperatures were examined by FE-SEM in detail, typical examples of which are shown in **Figure 9**. The fracture topography of the post-test specimen at RT is different from that at elevated temperature, depending on test temperature. At RT (Fig. 9a), the TS composite failed in a predominantly transgranular manner, with a trace amount of smaller TaB_2 grains that fractured in the intergranular fracture manner (indicated by arrows in Fig. 9a). At or above 1400°C, however, the TS composite failed in a predominantly intergranular manner (60~70% of the grains, Fig. 9b and c). In contrast, a few larger TaB_2 grains fractured in a transgranular manner (indicated by arrows in Fig. 9b and c). For the post-test specimen at 1500°C, particularly, the intergranular fracture manner is more pronounced (Fig. 9c), accompanying the protruding grains and open sockets left by grain pull out. The fracture mechanism transition from transgranular to intergranular manner indicated that the intergranular bonding significantly degraded at or above 1400°C. Under higher-magnification FE-SEM observation, no trace of grain boundary sliding along the glassy phase and cavitation were observed for the post-test specimen at 1500°C (Fig. 9d), however. The absence of grain boundary sliding and/or cavitation implies that the creep due to grain boundary sliding, which has a detrimental effect on the strength, could be minimized or neglected. Hence, the plastic flow of the materials due to the plastic deformation of TaB_2 grains, which accompanies the stress relief, contributed to the increase in the strength at or above 1400°C (Fig. 7).

In the case of TS3Y and TS3LA, on the other hand, the fracture topographies of the specimens at or below 1400°C are essentially similar to those of TS specimens; the two composites showed a rough fracture surface, with trace of slow crack growth after origination of crack from the flaws (Fig. 8d, e, g and h). In particular, the post-test two composites at RT exhibited the substantially rough fracture surfaces compared to TS specimen (Fig. 8a, d and g). However, their fracture surfaces at 1500°C are considerable flat and smooth character (Fig. 8f and i), in the absence of the SCG region. The absence of the SCG region implies that once the crack originates from the flaws at the surface and/or subsurface, the crack rapidly propagated until fracture of specimen.

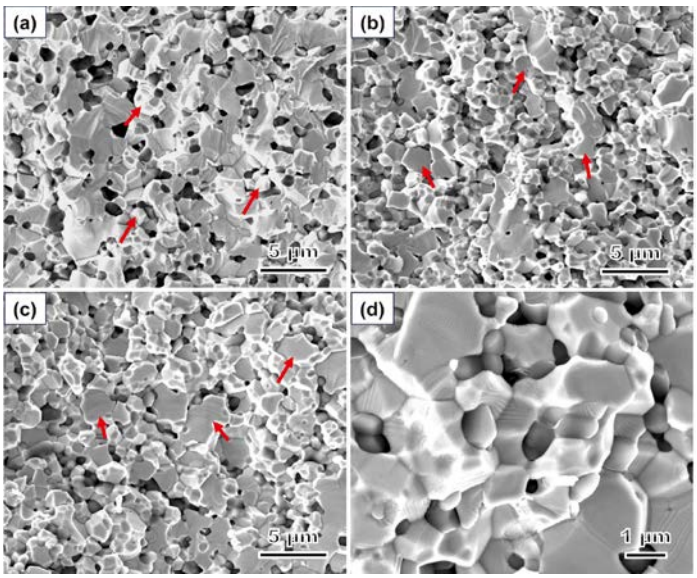

Fig. 9 FE-SEM images of the fracture surfaces for the post-test TS specimens at (a) RT, (b) 1400°C and (c, d) 1500°C.

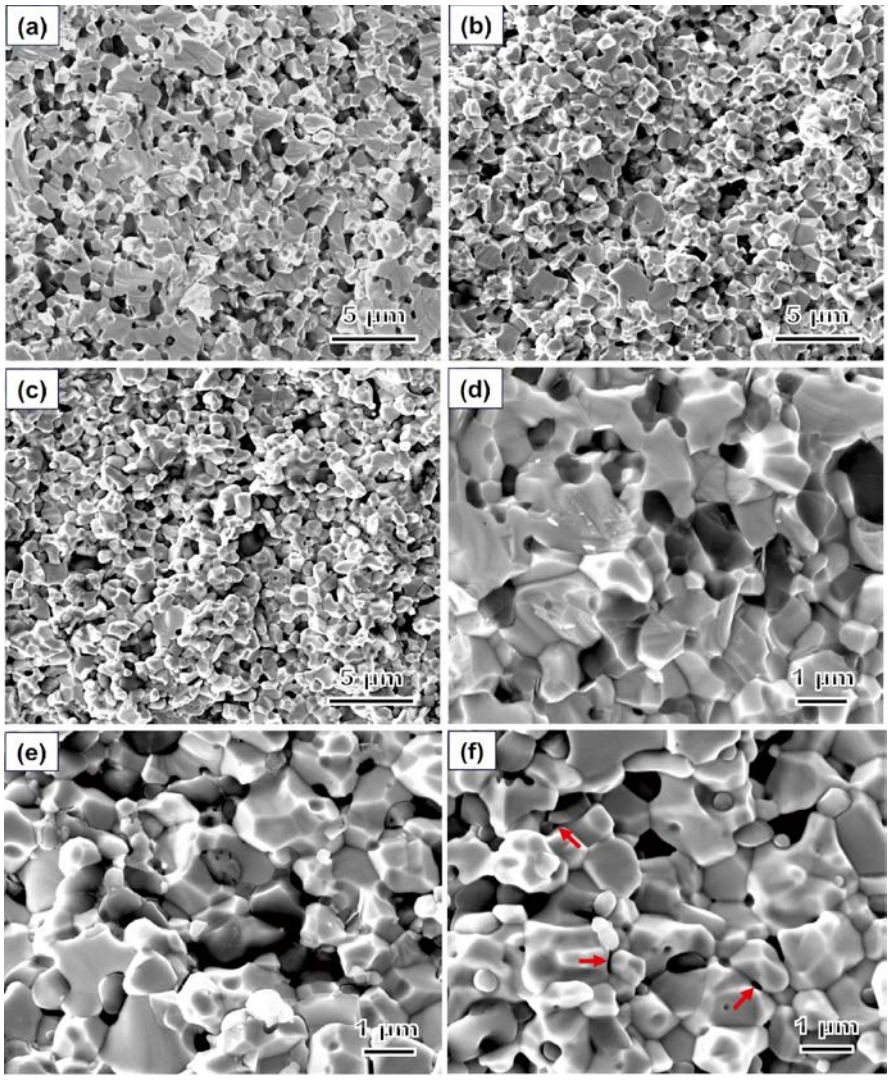

Fig. 10 FE-SEM images of the fracture surfaces for the post-test TS3Y specimens at (a, d) RT, (b, e) 1400°C and (c, f) 1500°C; (a–c) low-magnification and (d–f) higher-magnification.

The further FE-SEM observations of the fracture surfaces exhibited that the two composites failed in a predominantly transgranular manner at RT (**Fig. 10**a and **Fig. 11**a). Higher-magnification FE-SEM observations clearly showed a strong intergranular bonding for TS3Y and TS3LA (Fig. 10d and Fig. 11d), with no intergranular sliding or intergranular debonding. However, the predominant fracture mechanism transitioned from transgranular fracture at RT to intergranular fracture at or above 1400°C (≥80% of the grains, Fig. 10b and c, Fig. 11b and c), regardless of the type of RE_2O_3 additives. Compared to the TS composite without RE_2O_3 (Fig. 9b and c), the intergranular fracture manner is more pronounced for the TS3Y and TS3LA composites (Fig. 10b and c, Fig. 11b and c). In particular, the post-test specimens at 1500°C exhibited almost completely intergranular fracture for both the composites (Fig. 10c and Fig. 11c); this is attributed to the substantially softening of the intergranular glassy phase at 1500°C. As a result, a large amount of nonlinear deformation prior to fracture was observed in the stress-displacement curves obtained at 1500°C for TS3Y and TS3LA (Fig. 6b and c). Additionally, under higher-magnification FE-SEM observations (Fig. 10e and f, Fig. 11e and f), the protruding TaB_2 grains and open sockets left by grain pull out as well as intergranular debonding are clearly observed for the post-test TS3Y and TS3LA specimens at or above 1400°C; this indicates that the intergranular bonding substantially

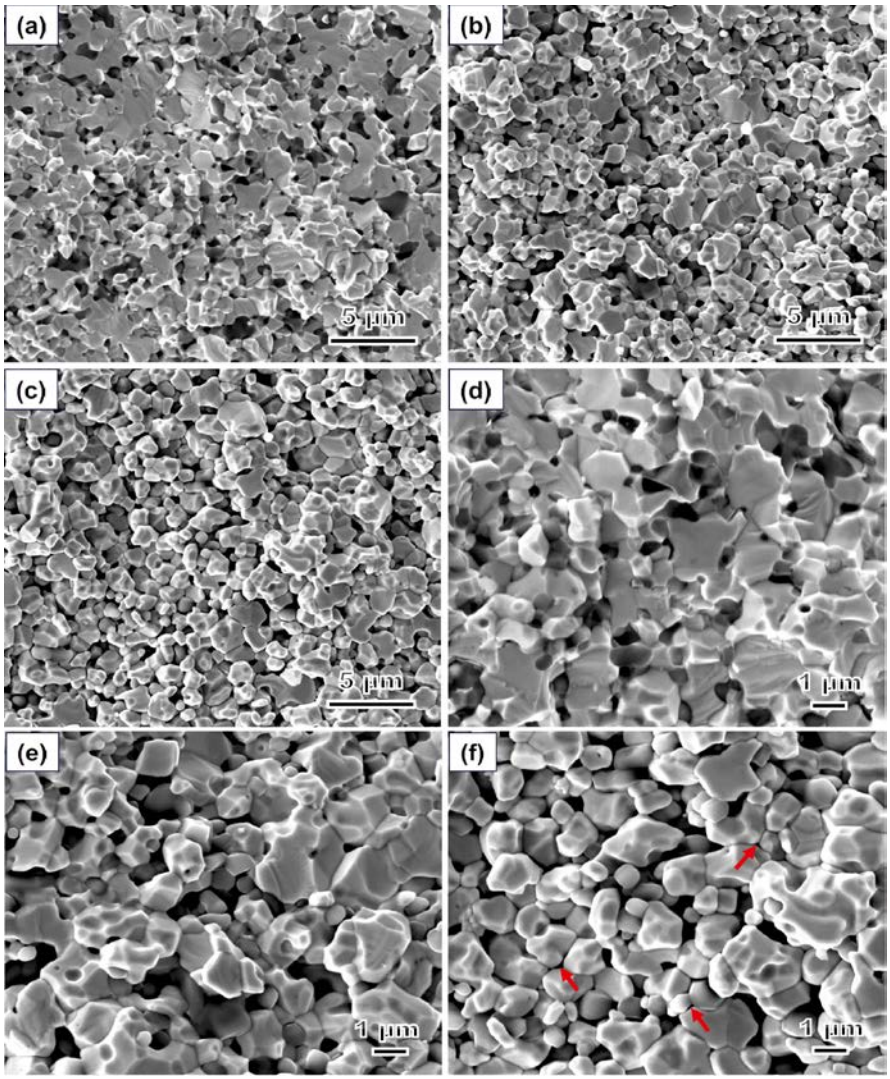

Fig. 11 FE-SEM images of the fracture surfaces for the post-test TS3LA specimens at (a, d) RT, (b, e) 1400°C and (c, f) 1500°C; (a–c) low-magnification and (d–f) higher-magnification.

degraded at or above 1400°C due to softening of the intergranular glassy phase. In particular, the post-test specimens at 1500°C exhibited the presence of the cavities at two grains boundaries (indicated by arrows in Fig. 10f and Fig. 11f), as a result of grain boundary sliding at high temperature, accommodated by viscous flow of the intergranular glassy phase at the grain boundaries. The grain-boundary sliding and generation of the cavities at two grains boundaries suggests the occurrence of creep at 1500°C for TS3Y and TS3LA specimens. Similarly, the generation and growth of cavitations due to grain-boundary sliding was reported by Guo et al. [42] in four-point flexural post-creep of ZrB_2-30 vol% SiC composite at or above 1500°C under a static load of 19 MPa in Ar. The occurrence of creep suggests that the intergranular glassy phase had a lower resistance to shear for TS3Y and TS3LA than for TS, as a result of the difference in the intergranular phase chemical compositions accompanied the additions of RE_2O_3. Thus, the creep having a detrimental effect on the strength could not be neglected, which led to the considerable nonlinear deformation (Fig. 6b and c) and substantially degradation of strength at 1500°C for TS3Y and TS3LA (Fig. 7), unlike TS where a few nonlinear deformations (Fig. 6a) and an increase of strength were observed (Fig. 7) owing to the absence of creep. Obviously, further examination is needed for understanding the effect of the intergranular phase chemistry on the microstructure and the mechanical properties.

4. Conclusions

The three compositions TaB_2-20 vol% SiC composites with and without 3 vol% RE_2O_3 (RE = Y and La) additives were fabricated via hot-pressing at different temperatures between 1800°C and 1900°C. The microstructure and mechanical properties of the resulting highly-dense composites were examined. The major results are drawn below.

(1) Relative density having higher than 96% was obtained at 1900°C for TS. Doped with 3 vol% RE_2O_3, relative density of > 96% was obtained at 1800°C for TS3Y and TS3LA.

(2) The resulting composites consisted of TaB_2 and SiC for TS, TaB_2, SiC and $Y_2Si_2O_7$ for TS3Y, and TaB_2, SiC and $La_2Si_2O_7$ for TS3LA. Additionally, the additions of RE_2O_3 significantly inhibited TaB_2 and SiC grain growth during the sintering process.

(3) The additions of RE_2O_3 led to reduction of the shear and Young's moduli as well as hardness. Conversely, the fracture toughness increased with the RE_2O_3 additives, and the toughening effect was higher for La_2O_3 than for Y_2O_3.

(4) At or below 1400°C, for TS only linear deformation behaviour was observed prior to fracture. At 1500°C, however, the initial linear response was followed by nonlinear deformation behaviour. In contrast, for TS3Y and TS3LA the nonlinear deformation behaviour was observed at or above 1400°C.

(5) At a temperature equal to or lower than 1200°C, the additions of RE_2O_3 significantly increased the flexural strength of TS, and the strengthening effect was significantly stronger for Y_2O_3 than for La_2O_3. At 1400°C, however, the strengths of the three compositions TS, TS3Y and TS3LA composites were comparable. Conversely, at 1500°C the strength of TS was substantially higher than that of TS3Y and TS3LA

(6) For TS without RE_2O_3 additives, the flexural strength was almost constant between RT and 1200°C, subsequently the strength increased with increase of temperature up to 1500°C. For TS3Y and TS3LA, the strengths increased with temperature up to 1000°C, the strengths degraded then with further increase temperature up to 1500°C. At a temperature lower than 1400°C, the strength was higher for TS3Y than for TS3LA. At or above 1400°C, however, the flexural strengths were almost the same for TS3Y and TS3LA.

Acknowledgments

This work is based on results obtained from a project, JPNP22005, commissioned by the New Energy and Industrial Technology Development Organization (NEDO).

References

[1] J. Castaing, P. Costa, Properties and Uses of Diborides in Boron and Refractory Borides edited by V.I. Matkovich, Springer Berlin Heidelberg, Berlin, Heidelberg, 1977, pp. 390–412.

[2] K. Nakano, Crystal structures and properties of borides, Bull. Ceram. Soc. Jap. 24 (1989) 500–508.

[3] X. Zhang, G.E. Hilmas, W.G. Fahrenholtz, Synthesis, densification, and mechanical properties of TaB_2, Mater. Lett. 62 (2008) 4251–4253.

[4] M.J. Gasch, D.T. Ellerby, S.M. Johnson, Ultra High Temperature Ceramic Composites in Handbook of Ceramic Composites edited by N.P. Bansal, Springer US, Boston, MA, 2005, pp. 197–224.

[5] W.G. Fahrenholtz, A historical perspective on research related to ultra-high temperature ceramics in Ultra-High Temperature Ceramics: Materials for Extreme Environment Applications edited by W.G. Fahrenholtz, E.J. Wuchina, W.E. Lee, Y. Zhou, The American Ceramic Society, 2014, pp. 6–32.

[6] D. Sciti, L. Silvestroni, J.-L. Sans, L. Mercatelli, M. Meucci, E. Sani, Tantalum diboride-based ceramics for bulk solar absorbers, Sol. Energy Mat. Sol. Cells 130 (2014) 208–216.

[7] G.A. Elliot, H.W. Lavendel, Sintering of TaB_2 in Sintering and Related Phenomena edited by G.C. Kuczynski, Gordon and Breach Science Publishers, New York 1967, pp. 565–579.

[8] H. Itoh, Y. Satoh, S. Kodama, S. Naka, Synthesis of tantalum boride powder by solid state reaction and its sintering, J. Ceram. Soc. Jpn. 98 (1990) 264–268.

[9] J. Matsushita, G.C. Hwang, K.B. Shim, Oxidation behavior of tantalum boride ceramics, Solid State Phenomena 124–126 (2007) 819–822.

[10] H. Lv, M. Ge, H. Zhang, H. Zhang, X. Sun, S. Yu, W. Zhang, High temperature oxidation behavior and mechanism of SiC-TaB_2 composites, J. Alloys Compd. 931 (2023) 167500.

[11] S.J. Lee, S.S. Baek, E.S. Kang, S.M. Yong, D.K. Kim, Fabrication and oxidation behaviour of reactive hot-pressed TaB_2-SiC ceramics, Rev. Adv. Mater. Sci. 28 (2011) 21–25.

[12] R. Licheri, R. Orru, C. Musa, G. Cao, Synthesis, densification and characterization of TaB_2-SiC composites, Ceram. Int. 36 (2010) 937–941.

[13] R. Licheri, R. Orru, C. Musa, G. Cao, Efficient technologies for the fabrication of dense TaB_2-based ultra-high-temperature ceramics, ACS Appl. Mater. Interfaces 2 (2010) 2206–2212.

[14] L. Silvestroni, S. Guicciardi, C. Melandri, D. Sciti, TaB_2-based ceramics: Microstructure, mechanical properties and oxidation resistance, J. Eur. Ceram. Soc. 32 (2012) 97–105.

[15] X. Ren, J. Lv, W. Li, Y. Hu, K. Sun, C. Ma, H. Chu, W. Wang, L. Xu, Z. Li, P. Feng, Influence of $MoSi_2$ on oxidation protective ability of TaB_2-SiC coating in oxygen-containing environments within a broad temperature range, J. Adv. Ceram. 9 (2020) 703–715.

[16] D.D. Jayaseelan, E. Zapata-Solvas, P. Brown, W.E. Lee, In situ formation of oxidation resistant refractory coating on SiC-reinforced ZrB_2 ultra high temperature ceramics, J. Am. Ceram. Soc. 95 (2012) 1247–1254.

[17] E. Zapata-Solvas, D.D. Jayaseelan, P.M. Brown, W.E. Lee, Effect of La_2O_3 addition on long-term oxidation kinetics of ZrB_2-SiC and HfB_2-SiC ultra-high temperature ceramics, J. Eur. Ceram. Soc. 34 (2014) 3535–3548.

[18] S.Q. Guo, Physical and mechanical behaviours of hot-pressed TaC-HfC ceramics with La_2O_3 additive, Adv. Appl. Ceram. 120 (2021) 117–126.

[19] S.Q. Guo, G. Okuma, K. Naito, H. Kakisawa, Mechanical behaviours of hot-pressed 4TaC-1ZrC ceramics with and without Y_2O_3 and La_2O_3 additives, Int. J. Refract. Met. Hard Mater. 117 (2023) 106389.

[20] X.H. Zhang, X.Y. Li, J.C. Han, W.B. Han C.Q. Hong, Effects of Y_2O_3 on microstructure and

mechanical properties of ZrB_2-SiC ceramics, J. Alloys Compd., 465 (2008) 506–511.
[21] M.I. Mendelson, Average grain size in polycrystalline ceramics, J. Am. Ceram. Soc. 52 (1969) 443–446.
[22] S.Q. Guo, N. Hirosaki, Y. Yamamoto, T. Nishimura, M. Mitomo, Hot-press sintering silicon nitride with Lu_2O_3 addition: Elastic moduli and fracture toughness, J. Eur. Ceram. Soc. 23 (2003) 537–545.
[23] G.R. Anstis, P. Chantikul, B.R. Lawn, D.B. Marshall, A critical evaluation of indentation techniques for measuring fracture toughness. I. Direct crack measurements, J. Am. Ceram. Soc. 64 (1981) 533–538.
[24] M. Keppeler, H.G. Reichert, J.M. Broadley, G. Thurn, I. Wiedmann, F. Aldinger, High temperature mechanical behaviour of liquid phase sintered silicon carbide, J. Eur. Ceram. Soc. 18 (1998) 521–526.
[25] Y.W. Kim, Y.S. Chun, T. Nishimura, M. Mitomo, Y.H. Lee, High-temperature strength of silicon carbide ceramics sintered with rare-earth oxide and aluminum nitride, Acta Mater. 55 (2007) 727–736.
[26] S.Q. Guo, Oxidation and strength retention of HfB_2-SiC composite with La_2O_3 additives, Adv. Appl. Ceram. 119 (2020) 218–223.
[27] S.K. Kashyap, K. Sala, R. Mitra, Oxidation resistance and evolution of multi-layered oxide scale during isothermal and cyclic exposure of ZrB_2-SiC-LaB_6 composites at 1300°C to 1500°C, Metall. Mater. Trans. A 53A (2022) 147–171.
[28] S.Q. Guo, Effects of VC additives on densification and elastic and mechanical properties of hot-pressed ZrB_2-SiC composites, J. Mater. Sci. 53 (2018) 4010–4021.
[29] W.G. Fahrenholtz, G.E. Hilmas, I.G. Talmy, J.A. Zaykoski, Refractory diborides of zirconium and hafnium, J. Am. Ceram. Soc. 90 (2007) 1347–1364.
[30] F. Monteverde, C. Melandri, S. Guicciardi, Microstructure and mechanical properties of HfB_2 + 30 vol% SiC composite consolidated by spark plasma sintering, Mater. Chem. Phys. 100 (2006) 513–519.
[31] Z. Sun, Y. Zhou, J. Wang, M. Li, γ-$Y_2Si_2O_7$, a machinable silicate ceramic: Mechanical properties and machinability, J. Am. Ceram. Soc. 90 (2007) 2535–2541.
[32] S.Q. Guo, T.W. Liu, D.H. Ping, T. Nishimura, Enhanced high-temperature strength of HfB_2-SiC composite up to 1600°C, J. Eur. Ceram. Soc. 38 (2018) 1152–1157
[33] S.Q. Guo, High-temperature mechanical behaviour of ZrB_2-based composites with micrometer- and nano-sized SiC particles, J. Am. Ceram. Soc. 101 (2018) 2707–2711.
[34] Y. Zhou, K. Hirao, M. Toriyama, Y. Yamauchi, S. Kanzaki, Effects of intergranular phase chemistry on the microstructure and mechanical properties of silicon carbide ceramics densified with rare-earth oxide and alumina additions, J. Am. Ceram. Soc. 84 (2001) 1642–1644.
[35] J. Zou, G.J. Zhang, C.F. Hu, T. Nishimura, Y. Sakka, H. Tanaka, J. Vleugels, O. Van der Biest, High-temperature bending strength, internal friction and stiffness of ZrB_2-20 vol% SiC ceramics, J. Eur. Ceram. Soc. 32 (2012) 2519–2527.
[36] S.Q. Guo, J.-M. Yang, H. Tanaka, Y. Kagawa, Effect of thermal exposure on strength of ZrB_2-based composites with nano-sized SiC particles, Compos. Sci. Technol. 68 (2008) 3033–3040.
[37] S. Zhu, W.G. Fahrenholtz, G.E. Hilmas, Influence of silicon carbide particle size on the microstructure and mechanical properties of zirconium diboride-silicon carbide ceramics, J. Eur. Ceram. Soc. 27 (2007) 2077–2083.
[38] A. Rezaie, W.G. Fahrenholtz, G.E. Hilmas, Effect of hot-pressing time and temperature on the microstructure and mechanical properties of ZrB_2-SiC, J. Mater. Sci. 42 (2007) 2735–2744.

[39] E.W. Neuman, G.E. Hilmas, W.G. Fahrenholtz, Mechanical behaviour of zirconium diboride-silicon carbide ceramics at elevated temperature in air, J. Eur. Ceram. Soc. 33 (2013) 2889–2899.
[40] W.A. Sanders, D.M. Mieskowski, Strength and microstructure of sintered Si_3N_4 with rare-earth-oxide additives, Am. Ceram. Soc. Bull. 64 (1985) 304–309.
[41] J. Watts, G. Hilmas, W.G. Fahrenholtz, D. Brown, B. Clausen, Stress measurements in ZrB_2-SiC composites using Raman spectroscopy and neutron diffraction, J. Eur. Ceram. Soc. 30 (2010) 2165–2171.
[42] W.M. Guo, G.J. Zhang, H.T. Lin, High-temperature flexural creep of ZrB_2-SiC ceramics in argon atmosphere, Ceram. Int. 38 (2012) 831–835.